EAST EUROPEAN JOURNAL OF PHYSICS. 2. 119-130 (2025)
DOI:10.26565/2312-4334-2025-2-12 ISSN 2312-4334

COMPARISON OF CORE AND NO-CORE SHELL MODELS IN EXCITATION OF NEGATIVE PARITY STATES OF $^{19}_{9}F$

Berun N. Ghafoor[a,c]*, Aziz H. Fatah[b#], Ari K. Ahmed[a§]
[a]*University of Sulaimani, College of Education, Physics department, Iraq*
[b]*University of Sulaimani, College of Science, Physics department, Iraq*
[c]*Research and Development Center, University of Sulaimani, Iraq*
**Corresponding Author e-mail: berun.ghafoor@univsul.edu.iq; [#]aziz.fatah@univsul.edu.iq; [§]ari.ahmed@univsul.edu.iq*
Received March 3, 2025; revised May 7, 2025; accepted May 8, 2025

The present study investigates the nuclear structure of low-lying negative parity states in $^{19}_{9}F$ using a combination of the shell model and Hartree-Fock (HF) approaches. A comprehensive analysis of nuclear properties—including energy spectra, electron scattering form factors, transition strengths, binding energies, and charge radii—was performed within four model spaces: the $sdpf$-model space, the zbm-model space, the psd-model space, and the extended $spsdpf$ no-core shell model space. Various effective interactions were applied within each model space to assess their impact on nuclear behavior. The HF method, utilizing multiple Skyrme parameterizations, along with harmonic oscillator and Woods-Saxon potentials, was employed to compute single-particle radial wave functions essential for matrix element calculations. The results demonstrate that Skyrme-based HF calculations, when integrated with shell model techniques, effectively capture fundamental nuclear properties. A systematic comparison with experimental data reveals that transitioning from core-restricted model spaces to a fully no-core framework significantly improves the reproduction of electron scattering form factors, particularly in both longitudinal (C1, C3) and transverse (E1, M2) components. Notably, specific states exhibit optimal agreement at different core levels: the $3/2^-_1$ and $5/2^-_1$ states are best reproduced in the no-core shell model, while the $7/2^-_1$ state achieves high accuracy within the zbm and psd model spaces. Overall, this research underscores the critical influence of model space selection and interaction choice in theoretical nuclear studies. The progressive refinement from core-based to no-core calculations highlights the role of many-body correlations in nuclear excitations and provides deeper insight into the intrinsic structure of $^{19}_{9}F$, contributing to advancements in nuclear structure theory and reaction dynamics.
Keywords: *Nuclear Structure; Model Spaces; Core-to-no-Core; Skyrme-HF; Fluorine-19*
PACS: 21.60.Cs, 21.60.Jz, 25.30.Bf, 21.10.-k, 27.20.+n

1. INTRODUCTION

Electron scattering, which involves the interaction of electrons with the nucleus via electromagnetic forces, is an important tool for studying nuclear structure, providing vital experimental data for testing theoretical models [1]. Its efficiency stems from the well-established electromagnetic interaction, which is properly characterized by quantum electrodynamics, as well as the interaction's relative weakness.

In this work, elastic and inelastic scattering form factors were estimated using the shell model and Hartree-Fock theory to produce single-particle states. The Hartree-Fock technique, a variational approach, generates the wave function of many-body quantum systems by modeling fermions as Slater determinants and bosons as product wave functions, assuring accurate statistical behavior during particle exchange [2].

The extension from core to no-core calculations is an important and effective method for reproducing accurate theoretical results in the present study. This technique focuses on increasing the number of valence particles to investigate the static and dynamic structure of $^{19}_{9}F$. Brown et al. (1985) [3] analyzed high-resolution electron scattering data for $^{19}_{9}F$, using the sd-model space for positive-parity states and the zbm-model space for both positive- and negative-parity. Their analysis of form factors and transition matrix elements demonstrated the utility of configuration mixing, although the interaction parameters available at the time limited the ability to fully capture complex nuclear dynamics.

Sakuda (1992) [4] analyzed the form factors of $^{19}_{9}F$ using a cluster model that combined the $(t + {}^{16}_{8}O)$ and $(\alpha + {}^{15}_{7}N)$ configurations. The framework appropriately compatible with experimental data for the magnetic form factor of the $\frac{1^+}{2}$ ground state, relying on significant cluster parts to imitate its three maxima. However, it demonstrated little agreement during the longitudinal form factors of the $\frac{5^-}{2}$, $\frac{7^-}{2}$, and $\frac{9^-}{2}$ states. The difference highlighted the need for future theoretical advances.

Elastic and inelastic electron scattering of $^{19}_{9}F$ was utilized [5] to investigate transitions from $1/2^+$ to $(1/2^+, 3/2^+, 5/2^+, 7/2^+, and\ 9/2^+)$. For all transitions considered in the study, the isospin value was $1/2$. The researchers employed the OXBASH package program code to generate the one-body density matrix (OBDM) with a large basis truncation of $(0 + 2)\hbar\omega$ for the harmonic oscillator potential in the $spsdpf$-model space. Subsequently, all form factors were computed using specific codes written in FORTRAN. A large basis was consistently applied throughout the study.

In the context of studying the influence of shell model interactions on weakly interacting massive particles (WIMPs), R. Abdel Khaleq et al. [6] utilized the sd-model space, incorporating USD and USDB interactions. This methodology

Cite as: B.N. Ghafoor, A.H. Fatah, A.K. Ahmed, East Eur. J. Phys. 2, 119 (2025), https://doi.org/10.26565/2312-4334-2025-2-12

enabled the calculation of energy levels and reduced transition probabilities for $^{19}_{9}F$, with single-particle states $1d_{5/2}$, $2s_{1/2}$ and $1d_{3/2}$ considered for both protons and neutrons.

In 2016, Radhi et al. [7] investigated inelastic electron scattering inside $^{19}_{9}F$ using shell model calculations for both positive and negative parity states. Their research of positive parity states used the sd-model space with USDA interaction and focused on a selection of energy levels.

Elastic and inelastic scattering, energy levels, and reduced transition probabilities for specific positive and negative parity states were investigated using the nuclear shell model [7]. The sd-model space was employed for positive parity states, while the $spsdpf$ model space, truncated with$(0 + 2)\hbar\omega$, was applied for negative parity states. Although their work represents a significant contribution, certain limitations remain, particularly in the treatment of the $M3$ and E4 components. This highlights the necessity of extending the model spaces to achieve higher precision in future studies.

The present investigation evaluates the energy spectra, reduced transition probabilities, magnetic dipole moments, nuclear root-mean-square radii, binding energy, and both longitudinal and transverse inelastic electron scattering form factors for the negative parity states of $^{19}_{9}F$ nucleus. The analysis utilizes four distinct model spaces to systematically examine the influence of progressively extending the core configuration, culminating in a no-core framework, on the calculated nuclear properties and scattering observables. All types of model space Hamiltonians have been utilized to generate realistic wave functions for the negative-parity states of $^{19}_{9}F$, including the $1/2^-$ at 0.1098MeV, $3/2^-_1$ at 1.459 MeV, $5/2^-_1$ at 1.3465MeV, and $7/2^-_1$ at 3.9987MeV.

The first approach is for $sd - pf$ shell called $sdpf$-model space, incorporating the active $1d_{5/2}$, $2s_{1/2}$ and $1d_{3/2}$ orbitals above an inert $^{16}_{8}O$ core, treated as closed in the $(1s)^4(1p)^{12}$ configuration. The next model space, designated as Zuker–Buck–McGrory (zbm-model space), includes the active $1p_{1/2}$, $1d_{5/2}$, and $2s_{1/2}$ orbitals positioned above an inert $^{12}_{6}C$ core. To accurately represent the complicated nuclear dynamics inside this approach, zbm-model space interactions, such as Zuker–Buck–McGrory-Interaction (ZBMI) [8] and Zuker-MCGRORY-WILDENTHAL (ZWM) [9], were used to create exact wave functions for the respective states.

The $p - sd$ orbits employ $psdpn$-model space [10] includes active shells $1p_{1/2}, 1p_{3/2}, 1d_{3/2}, 1d_{5/2}, and\ 2s_{1/2}$ above the inert $^{4}_{2}He$ nucleus core, where the $(1s)^4$ configuration remains closed. This model space features center-of-mass motion and $p - sd$ orbits employ psd-model space interactions, such as PSDMK and PSDMWK, to connect the p- and sd-model spaces. The PSDMK interaction [11] comes from the pw-interaction inside the sd-model space. It contains the active $1d_{5/2}$, $2s_{1/2}$, and $1d_{3/2}$ orbitals atop an inert $^{16}_{8}O$ core. Furthermore, the p-model space, with the Cohen-Kurath- POT ($CKPOT$) interaction [12], involves the $1p_{1/2}$, and $1p_{3/2}$ orbitals above the inert $^{4}_{2}He$ core. The last model space was used in present study known as $spsdpf$ includes active orbitals $1s_{1/2}$, $1p_{3/2}$, $1p_{1/2}$, $1d_{5/2}$, , $1d_{3/2}$, $2s_{1/2}$, $1f_{7/2}$, $1f_{5/2}$, $2p_{3/2}$, and $2p_{1/2}$, covering four major shells: $1s, 1p, 2s - 1d, and\ 1f - 2p$ with specific truncations. Considering no combination of $n\hbar\omega$ and $(0 + 2)\hbar\omega$ configurations, the model's interactions, created by Warburton and Brown [13], are based on a least-squares fit to 216 energy levels in the $A = 10–22$ area. With two body matrix element (TBME) and single particle energies (SPE) fitted for the p-shell and then expanded to include the $1s$ and $2p1f$ shells, the Warburton–Becker (WBT and WBP) interactions were used. The Warburton–Becker–Milliner–Brown (WBMB) interaction was used to represent cross-shell interactions [14].

The Skyrme Hartree–Fock (SHF) method, grounded in mean-field (MF) theory, has been utilized to compute single-particle matrix elements for excited nuclear states with various parameterizations. This approach minimizes the energy of a single Slater determinant derived from two-body interactions, offering an efficient solution through an analytic energy density functional for spherical nuclei [2, 15]. The SHF framework determines self-consistent potentials, single-particle densities, and minimal energy states, while also accommodating deformed or generalized bases for broader applications. Initially implemented by Vautherin and Brink, the Skyrme interaction has demonstrated significant success in nuclear MF calculations. Its parameterization, incorporating s- and p-wave expansions of effective nucleon–nucleon forces alongside density-dependent terms, captures critical nuclear physics, including shell-model truncations to closed-shell configurations and three-body effects [15]. As a phenomenological model, the parameters are refined against experimental data to ensure precision and reliability in predictive modeling [2].

2. THEORY AND METHODOLOGY

The reduced spin matrix element of electron–nucleus scattering between the initial and final nuclear states, $\langle J_i||\hat{T}^{\eta}_{J,t_z}(q)||J_f\rangle$, in the shell model framework is expressed as the sum of the one-body density matrix elements (OBDM) multiplied by the corresponding single-particle matrix elements of the transition operator, or

$$\langle J_i||\hat{T}^{\eta}_{J,t_z}(q)||J_f\rangle = \sum_{j_i,j_f} OBDM_{J,t_z}(j_i,j_f)\,\langle j_i||\hat{T}^{\eta}_{J,t_z}(q)||j_f\rangle. \quad (1)$$

Here J_i and J_f label initial and final nuclear states respectively and j_i and j_f label single-particle states for the shell model space. The symbol $\hat{T}^{\eta}$ is nuclear spins anyone of $\hat{T}^{Coulmb}$, $\hat{T}^{electric}$, or $\hat{T}^{magnetic}$ and $t_z = 1/2$ for a proton and $t_z = -1/2$ for a neutron

The electron scattering form factor has a longitudinal $F_L(q)$ and a transverse component, $F_T(q)$ and can be written in terms of reduced matrix elements of the electromagnetic transition operators of electron scattering, including the finite-size and center of mass correction form factors [1, 16]

$$|F_\eta^J(q)|^2 = \frac{4\pi}{Z^2(2J_i+1)} |\sum_{t_z} e(t_z)\langle J_f||\hat{T}^\eta_{J,t_z}(q)||J_i\rangle|^2 \times |F_{cm}(q)|^2|F_{fs}(q)|^2. \quad (2)$$

Here $F_\eta = F_{C,E,M}$ that is represents each of Coulomb, transverse electric and magnetic form factors. Since $Z\alpha \ll 1$, the electron scattering process can be accurately described using the plane-wave first-order Born approximation. In this approximation, the interaction is treated perturbatively, and the transition matrix elements are evaluated using the unperturbed nuclear states. Accordingly, the form factors presented in this work are computed within this approximation framework, which is valid for the kinematic conditions considered in this study [17, 18], with using Wigner-Eckart theorem [17] the total longitudinal (L)and transverse (T)form factors are given by

$$|F_L(q)|^2 = \frac{1}{2J_i+1}\sum_{J\geq 0} |\langle J_f||\hat{T}^{Coulomb}_{J,t_z}(q)||J_i\rangle|^2, \quad (3)$$

$$|F_T(q)|^2 = \frac{1}{2J_i+1}\sum_{J\geq 1}\{|\langle J_f||\hat{T}^{electric}_{J,t_z}(q)||J_i\rangle|^2 + |\langle J_f||\hat{T}^{magnetic}_{J,t_z}(q)||J_i\rangle|^2\}, \quad (4)$$

The total form factor can be expressed from the sum of its components [1]

$$|F(q,\theta)|^2 = (1-\omega^2/q^2)|F_L(q)|^2 + \left[\frac{1}{2}(1-\omega^2/q^2) + tan^2\frac{\theta}{2}\right]|F_L(q)|^2, \quad (5)$$

where θ is the electron scattering angle.

The Skyrme potential is employed as the central potential, characterized by its role as a mean-field potential. This potential approximates the collective effect of all nucleons within the nucleus, simulating the interactions among them while representing the realistic forces between nucleon pairs and triplets. Mathematically, the Skyrme interaction, V_{Skyrme}, is expressed as a combination of two-body and three-body components [2].

$$\hat{V}_{Skyrme} = \sum_{i<j} V^{(2)}_{ij} + \sum_{i<j<k} V^{(3)}_{ijk}. \quad (6)$$

The two-body part interaction also contains the mean central, spin-orbit, and the tensor parts. In momentum space it can be written as [18, 19]

$$\hat{V}_{Skyrme}(\boldsymbol{r_1}, \boldsymbol{r_2}) = \hat{V}^m + \hat{V}^{L.S} + \hat{V}^t. \quad (7)$$

Where

$$\hat{V}^m = t_0\big(1 + x_0\hat{P}_\sigma\big)\delta_{12} + \frac{t_1}{2}\big(1 + x_1\hat{P}_\sigma\big)\big(\hat{\boldsymbol{k}}_1^2 + \hat{\boldsymbol{k}}_2^2\big)\delta_{12} + t_2(1 + x_2\hat{P}_\sigma)\hat{\boldsymbol{k}}_2.\hat{\boldsymbol{k}}_1\delta_{12} + \frac{t_3}{6}(1 + x_3\hat{P}_\sigma)\rho^\alpha(\boldsymbol{r})\delta_{12}, \quad (8)$$

$$\hat{V}^{L.S} = it_4 + (\hat{\sigma}_1 + \hat{\sigma}_2).\hat{\boldsymbol{k}}_2 \times \hat{\boldsymbol{k}}_1\delta_{12}, \quad (9)$$

$$\hat{V}^t = \frac{t_e}{2}\{\big[3(\hat{\sigma}_1.\hat{\boldsymbol{k}}_2)(\hat{\sigma}_2.\hat{\boldsymbol{k}}_2) - (\hat{\sigma}_1.\hat{\sigma}_2)\hat{\boldsymbol{k}}_2^2\big]\delta_{12} + \big[3(\hat{\sigma}_1.\hat{\boldsymbol{k}}_1)(\hat{\sigma}_2.\hat{\boldsymbol{k}}_1) - (\hat{\sigma}_1.\hat{\sigma}_2)\hat{\boldsymbol{k}}_1^2\big]\delta_{12}\} + t_s\big[3(\hat{\sigma}_1.\hat{\boldsymbol{k}}_2)(\hat{\sigma}_2.\hat{\boldsymbol{k}}_1) - (\hat{\sigma}_1.\hat{\sigma}_2)\hat{\boldsymbol{k}}_2.\hat{\boldsymbol{k}}_1^2\big]\delta_{12}, \quad (10)$$

δ_{12} is the Dirac delta function, $\delta_{12} = \delta(\boldsymbol{r}_1 - \boldsymbol{r}_2)$, $\hat{\sigma}_1$ and $\hat{\sigma}_2$ are the vector of Pauli spin matrices for the first and second nucleon respectively, and three body part can be written as

$$V^{(3)}_{Skyrme} = t_3\delta_{12}\delta_{13}. \quad (11)$$

The $\hat{\boldsymbol{k}}_1$ and $\hat{\boldsymbol{k}}_2$ operators are the relative momentums, wave vectors, of the first and second nucleon which operate on the wave functions to the right $|\psi\rangle$ and to the left $\langle\psi|$ respectively and having the form

$$\hat{\boldsymbol{k}}_1 = \frac{1}{2i}\big(\vec{\nabla}_1 - \vec{\nabla}_2\big)\,,\ \hat{\boldsymbol{k}}_2 = -\frac{1}{2i}\big(\overleftarrow{\nabla}_1 - \overleftarrow{\nabla}_2\big)\,. \quad (12)$$

The reduced transition probability [1], representing the probability of a nuclear transition between states, is mathematically expressed as:

$$B(\eta J) = \frac{Z^2}{4\pi}\left[\frac{(2J+1)!!}{k^J}\right]^2 |F_J^\eta(k)|^2. \quad (13)$$

Here $k = \frac{E_x}{\hbar c}$

3. RESULT AND DISCUSSION

The study of nuclear electromagnetic form factors provides critical insights into the structural and dynamic properties of atomic nuclei. This work systematically examined the longitudinal and transverse form factors of $^{19}_{9}F$ for negative parity states through electron scattering, employing advanced shell-model techniques. Various model spaces

were utilized to highlight the effects of core extensions and model-space expansions. The $sdpf$-model space with $^{16}_{8}O$ as the core and SDPFK interaction focused on proton-neutron correlations, while the zbm-model space with a $^{12}_{6}C$ core explored configuration mixing in the p-shell via $ZBMI$ interaction. The psd-model space, based on a $^{4}_{2}He$ core, and the $spsdpf$ model space, treating all 19 nucleons as fully interacting, captured the nucleus's complete structure. Theoretical results were compared with experimental data to improve the influence of model-space truncation and interaction choices. One-body density matrix (OBDM) components, computed by using NuShellX@MSU [20], enabled calculation of MJ and EJ operators. Radial wave functions for single-particle matrix elements were generated using Skyrme-Hartree-Fock potentials ($SkXcsb, SkXta, SkXtb, and\ SLy4$), the Wood-Saxon potential, and a harmonic oscillator potential ($b = 1.833\ fm$) [3], facilitating a comprehensive model comparison. Utilizing the SLy4 parameterization, the computed root mean square (rms) charge radius was determined to be 2.876 fm, aligning well with the experimental measurement of 2.8976 fm [21]. Additionally, the binding energy calculation yielded 146.3719 MeV, exhibiting strong consistency with the experimental value of 147.803 MeV [22]. Furthermore, the nuclear magnetic dipole moment for the $5/2^-_1$ state was evaluated at 0.613 nm, which closely approximates the experimental determination of 0.67(11) nm [23-25].

Discussions of the results is organized systematically to provide a comprehensive understanding of the findings. The present analysis encompasses several key aspects: inelastic electron scattering form factors, energy level transitions and associated probabilities. These results are presented sequentially, following an order based on increasing angular momentum, offering a coherent narrative of the nuclear structure and dynamics under investigation.

3.1. The form factors

The current study utilized the $sdpf$-model space with the SDPFK two-body effective interaction [26], the zbm-model space with the ZBMI effective interaction [8], the psd-model space using the PSDMK effective interaction [11], and the $spsdpf$-model space with the WBT interaction to reproduce both longitudinal and transverse form factors. This approach was designed to highlight the effects of extending the core and to enable a comparative analysis between the different model spaces.

Based on the selection rules governing total angular momentum and parity conservation, the permissible multipole components for pure coulomb and transverse form factors are $C1$ and $E1$ respectively. The elastic Coulomb $C1$ form factors for the ground state of the $^{19}_{9}F$ nucleus $1/2^-$ were computed using wave functions from the $sdpf, zbm, psd,$ and $spsdpf$ model spaces, along with parameterizations from $Skxcsb, Skxta, Skxtb, Sly4,$ Wood-Saxon (WS), and harmonic oscillator (HO) potentials. The results, depicted in Fig. (1), are compared against experimental data from Ref. [1].

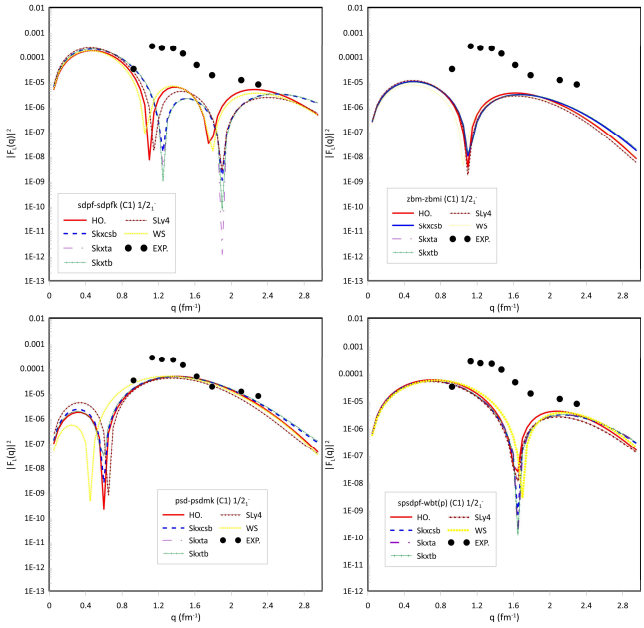

Figure 1. Theoretical longitudinal form factor $C1$ for $1/2^-_1$ compared with experimental data [3, 27]

The $sdpf$ model space, with $^{16}_{8}O$ as the core, effectively reproduces the C1 form factor at momentum transfer values of $q = 0.92\ fm^{-1}$ and $q = (2.00\ - 2.26) fm^{-1}$. However, in the intermediate range $q = (1.00 - 2.00) fm^{-1}$, while the qualitative agreement with experimental data remains reasonable, the quantitative agreement is notably poor due to the restricted participation of nucleons in the interaction. Conversely, employing the zbm model space with $^{12}_{6}C$ as the core results in a poor reproduction of the C1 form factor. This model exhibits a slight shift relative to the experimental data for $q = (0.90 - 2.00) fm^{-1}$. Nevertheless, at $q > 2.00\ fm^{-1}$, it achieves good agreement, particularly when using the $Skxcsb$ Skyrme potential. On the other hand, the psd model space, with $^{4}_{2}He$ as the core, successfully reproduces the C1 form factor both qualitatively and quantitatively across all types of potentials. Notably, at $q = 0.90\ fm^{-1}$, Wood-Saxon potential has a

significant influence in optimizing the reproduction of the form factor. Furthermore, within the range $q = (2.00 - 2.50) fm^{-1}$, the Skyrme interactions ($Skxcsb$ and $Skxtb$) play a crucial role in enhancing the accuracy of the form factor reproduction. Finally, employing the $spsdpf$ model space within a no-core shell model framework for C1 form factor calculations demonstrates that both potential types yield comparable results. The no-core shell model not only ensures a quantitatively accurate reproduction but also achieves the best agreement at both initial and final scattering points.

The calculated E1 form factors associated with the negative-parity state of $(1/2^-, 0.1098\ MeV)$ are presented in Fig. 2. The reproduction of the E1 form factor within the $sdpf$ model space using the SDPFK interaction exhibits overall poor agreement with experimental data. However, at specific momentum transfer values, such as $q = 0.78\ fm^{-1}$ and within the range $q = 1.00 - 1.20\ fm^{-1}$ reasonable agreement is observed, with the best reproduction occurring in the interval $q = (2.00 - 2.50)\ fm^{-1}$. For $q = (1.40 - 1.60)\ fm^{-1}$, the Harmonic Oscillator (HO) and Wood-Saxon (WS) potentials demonstrate a qualitatively satisfactory reproduction of the E1 form factor, while the SLy4 Skyrme interaction extends this agreement up to $q = 1.80\ fm^{-1}$. Expanding the core from ${}^{16}_{8}O$ to ${}^{12}_{6}C$ effectively resolves many discrepancies in reproducing the E1 form factor. By utilizing the zbm model space and ZBMI interaction for seven nucleons outside the core, the E1 form factors are successfully reproduced in good agreement with experimental data across all potential types examined in this study, except for the initial drop in the momentum transfer region.

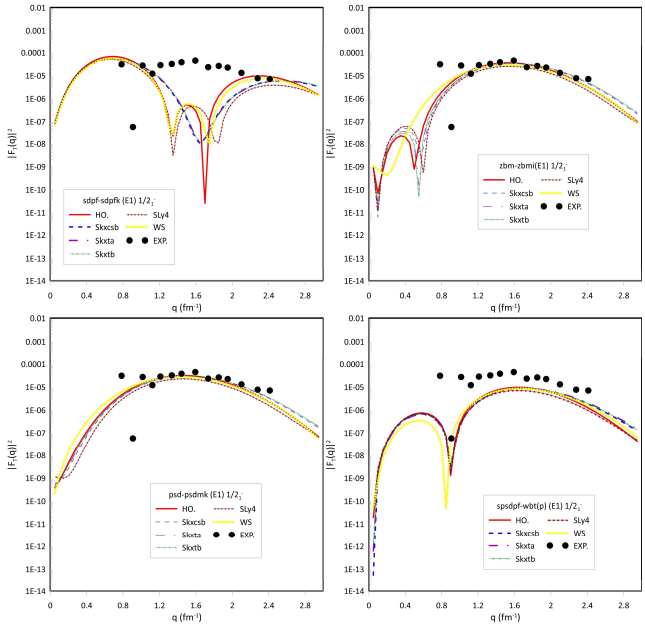

Figure 2. Theoretical transverse form factor $E1$ for $1/2_1^-$ compared with experimental data [3, 27]

Expanding the core to ${}^{4}_{2}He$ within the psd model space, incorporating fifteen interacting nucleons, yields an optimal reproduction of the E1 form factor, achieving both qualitative and quantitative agreement across the entire momentum transfer region. The only exception is the initial drop in the momentum transfer, which occurs within the scattering region. However, this discrepancy is effectively resolved through no-core shell model calculations. Furthermore, employing the no-core shell model with the $spsdpf$ model space, where all nucleons actively participate in the interaction, helps refine fluctuations in the scattering process. This highlights the significant impact of extending from a core-based framework to a no-core approach in enhancing the accuracy of form factor reproduction.

The C1 form factor for the negative-parity state $3/2_1^-$ (1.459 MeV) is depicted in Fig. (3). Within the $sdpf$ model space, which considers three interacting nucleons, the C1 form factor for this state exhibits three distinct scattering peaks, resulting in an overall quantitatively good agreement with experimental data. However, the first drop in the form factor occurs experimentally around $q = 1.76\ fm^{-1}$, whereas all potential types within this model space predict the decline at lower momentum transfer values. To address this fluctuation across all potential types, a second systematic peak rapidly emerges, aligning with the experimental momentum transfer points, particularly for the Harmonic Oscillator (HO) potential. The minor fluctuation preceding this peak also leads to a delayed reproduction of the second experimentally observed rising peak in theoretical calculations. Nevertheless, this state represents an extreme case, as previous theoretical studies by Brown et al. [3] and Donne et al. [28] exhibit significant deviations from experimental data.

Conversely, the zbm model space, with ${}^{12}_{6}C$ as the core, qualitatively reproduces the C1 form factor while maintaining the overall scattering shape. However, it exhibits systematic shifts, suggesting that the theoretical scattering process begins prematurely than observed experimentally. This discrepancy may be mitigated through minor parameter adjustments within the model space. In contrast, the psd model space, with ${}^{4}_{2}He$ as the core, successfully reproduces the C1 form factor up to the first drop in momentum transfer but fails to capture the second rising peak. Ultimately, the C1 form factor for the $3/2_1^-$ state achieves the highest qualitative agreement with experimental data [3] and exhibits good quantitative agreement when calculated using the $spsdpf$ model space within no-core shell model framework. Notably,

while R.A. Radhi et al. [7] previously reported that the C1 form factor for this state could not be reproduced using the no-core shell model, the present study demonstrates that no-core approach successfully achieves a strong agreement with experimental data.

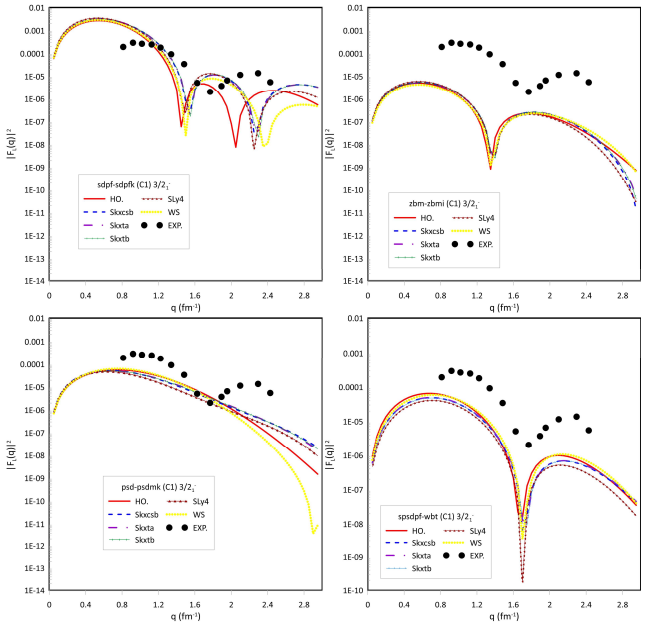

Figure 3. Theoretical longitudinal form factor $C1$ for $3/2_1^-$ compared with experimental data [3, 28]

The total form factor, incorporating both E1 and M2 contributions for the $3/2_1^-$ state, is illustrated in Fig. (4). The $sdpf$ model space achieves the best agreement within the momentum transfer range of $q = (1.40 - 1.60)\ fm^{-1}$, particularly when employing Harmonic Oscillator (HO), Wood-Saxon (WS), and SLy4 potential parameterizations.

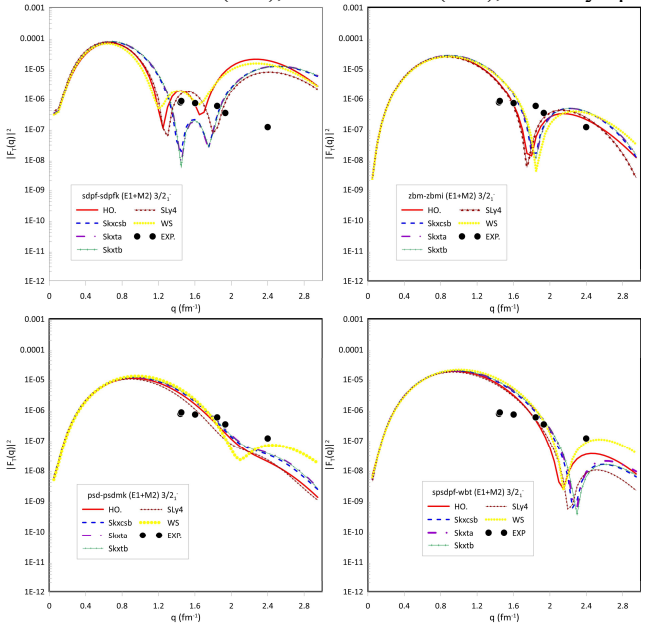

Figure 4. Theoretical Transverse form factors $E1, and\ M2$ for $3/2_1^-$, 1.459 MeV compared with experimental data [3, 28].

Additionally, for $q = (1.70 - 2.00)\ fm^{-1}$, Skyrme potentials—especially SkXcsb, SkXtab, and SkXtb—exhibit strong agreement with experimental data. However, at the end of scattering point near $q = 2.40\ fm^{-1}$, the $sdpf$ model space fails to accurately reproduce the form factor. In contrast, the zbm model space provides a quantitatively consistent reproduction of the total transverse form factor for this state, except at the peak near $q = 2.40\ fm^{-1}$. Both the psd model space (with ${}_2^4He$ as the core) and the $spsdpf$ no-core shell model successfully cover the entire momentum transfer range throughout the scattering process. Notably, they achieve the best agreement at the final experimental curvature point, $q = 2.40\ fm^{-1}$, particularly when using WS potential.

The C3 form factor for the $5/2_1^-$- state is depicted in Fig. 5. The $sdpf$ model space initially demonstrates a qualitatively good agreement in reproducing the form factor; however, near $q = 2.00\ fm^{-1}$, it exhibits fluctuations and rapidly declines.

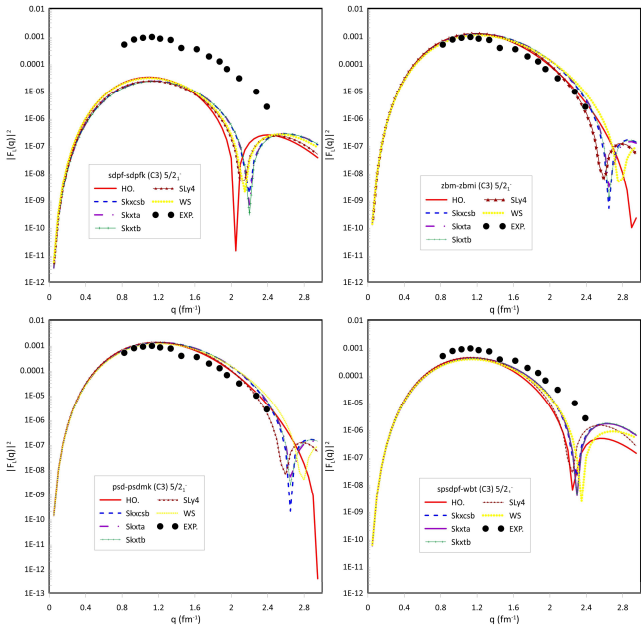

Figure 5. Theoretical longitudinal form factor $C3$ for $5/2_1^-$ compared with experimental data [3, 28].

In contrast, the zbm model space, incorporating seven interacting nucleons with the ZBMI interaction, successfully covers the entire momentum transfer range and accurately reproduces the C3 form factor both qualitatively and quantitatively across all potential parameterizations. Similarly, the psd model space, with ${}_2^4He$ as the core and the PSDMK interaction for fifteen nucleons, achieves the best agreement, particularly when using the Harmonic Oscillator (HO) potential and SLy4 Skyrme parameterization. Furthermore, the $spsdpf$ model space, employing WBT interaction within no-core shell model framework, reproduces the C3 form factor in good agreement, albeit with minor fluctuations around $q = 2.30\ fm^{-1}$.

The total transverse form factor for the $5/2_1^-$ state with (1.3456 MeV), which represents the combined contributions of M2 and E3, is illustrated in Fig. 6.

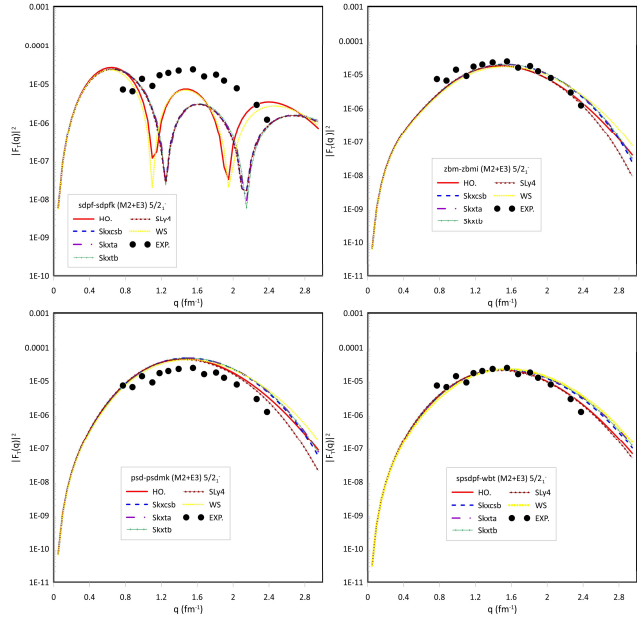

Figure 6. Theoretical transverse form factor $E3, and\ M2$ for $5/2_1^-, 1.3456\ MeV$ compared with experimental data [3, 28].

The $sdpf$ model space, incorporating only three interacting nucleons with ${}_8^{16}O$ as the core, demonstrates some capability in reproducing the form factor. However, it exhibits two significant fluctuations, characterized by rapid declines near $q = (0.80 - 1.20)\ fm^{-1}$ and $q = (1.80 - 2.20)\ fm^{-1}$, with variations depending on the potential type. In contrast, the zbm, psd, and $spsdpf$ model spaces achieve optimal agreement with experimental data, both qualitatively and quantitatively, effectively reproducing the form factor across the entire momentum transfer range.

The C3 form factor for the $7/2_1^-$ state is presented in Fig. 7. The $sdpf$ model space demonstrates a poor ability to reproduce the form factor, likely due to the limited number of nucleons involved in the interaction. This constraint causes

the theoretical scattering process to occur slightly earlier than the experimental results. Expanding the core to $^{12}_{6}C$ within the zbm model space and incorporating four additional nucleons significantly improves the agreement with experimental data, particularly in the end phase of the scattering process around $q = (2.00 - 2.40)\ fm^{-1}$, especially when employing Skyrme parameterizations. Similarly, the psd model space with a $^{4}_{2}He$ core produces a form factor that closely resembles the zbm model space results. This similarity arises from the structural equivalence of the $^{12}_{6}C$ core to three clustered $^{4}_{2}He$ nuclei in the context of this single-particle excitation state.

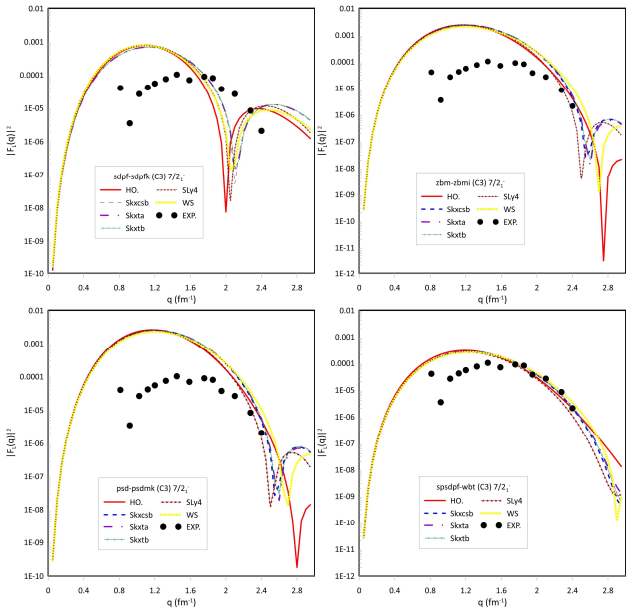

Figure 7. Theoretical longitudinal form factor $C3$ for $7/2^{-}_{1}$ compared with experimental data [3, 27].

The observed resemblance of the C3 form factor when using $^{12}_{6}C$ and $^{4}_{2}He$ as core nuclei indicates that the primary contribution originates from valence nucleons within the sd-shell, rather than from core excitations. Factors such as transition density, wavefunction overlap, and the minimal role of core excitation contribute to the nearly identical results across both model spaces. Furthermore, the $spsdpf$ model space, representing no-core shell model calculation, successfully reproduces the C3 form factor both qualitatively and quantitatively. This highlights the significance of transitioning from core-based to no-core calculations in achieving improved theoretical-experimental consistency.

The total transverse form factor for the $7/2^{-}_{1}$ state at 3.9987 MeV, comprising E3 and M4 contributions depicted in Fig. 8. The $sdpf$ model space successfully captures the qualitative features of the form factor within the momentum transfer range $q = (0.80 - 1.60)\ fm^{-1}$, though it fails to achieve quantitative agreement in this region. However, for $q = (1.60 - 2.10)\ fm^{-1}$, the model exhibits a strong correspondence with experimental data.

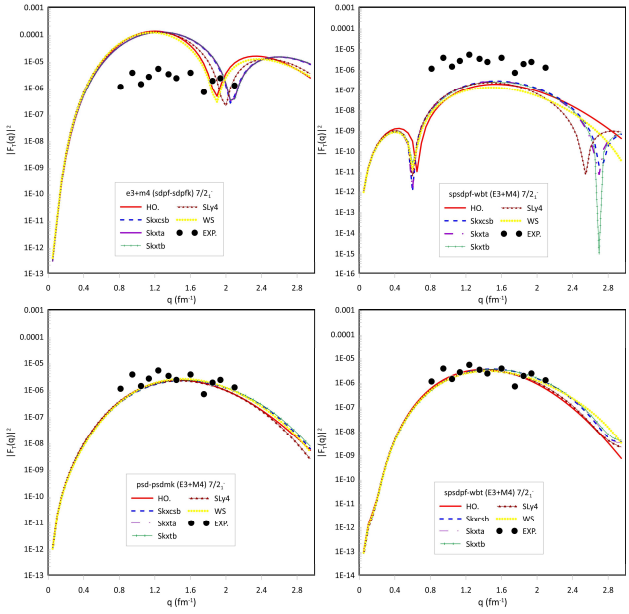

Figure 8. Theoretical transverse form factors $E3, and\ M4$ for $7/2^{-}_{1}, 3.9987\ MeV$ compared with experimental data [3, 28]

Conversely, the zbm model space effectively reproduces the total transverse form factor across the entire momentum transfer range, maintaining a high degree of qualitative accuracy. Nonetheless, it falls short in precisely matching the quantitative values of the experimental results, with a systematic discrepancy.

In contrast, both the psd model space with $^{4}_{2}He$ core and the $spsdpf$ model space (no-core shell model) demonstrate superior performance, successfully reproducing the form factor with high accuracy in both qualitative and quantitative aspects. This highlights the enhanced predictive capability of models incorporating extended nucleon interactions, particularly in no-core shell model calculations.

3.2. Energy levels

The negative parity energy levels of $^{19}_{9}F$ reveal a profound dependence on the choice of model space and interaction, reflecting the intricate many-body dynamics governing nuclear structure and illustrated in Fig. 9. The $sdpf$ model space with the SDPFK interaction with $^{16}_{8}O$ core provides an initial approximation but struggles to fully capture experimental trends due to its limited treatment of nucleon correlations. Extending the core to $^{12}_{6}C$ (zbm model space, ZBMI interaction) significantly refines the predictions, particularly for the $J^{\pi} = 9/2^{-}_{1}$ state, where the additional valence nucleons improve agreement with experimental data. The psd model space with PSDMK interaction with $^{4}_{2}He$ core introduces a different perspective by treating $^{12}_{6}C$ as three $^{4}_{2}He$ clusters, resulting in comparable C3 form factors and energy levels to the ZBM approach. However, the most striking improvement emerges in the no-core shell model ($spsdpf$ model space), where WBT and WBP interactions systematically reproduce the experimental spectrum with remarkable precision. This transition from a static core approximation to a fully correlated nucleonic treatment, highlights the essential role of many-body correlations, particularly in capturing the finer details of higher negative parity states.

The no-core shell model correctly reproduces both qualitative trends and quantitative values along with energy levels of $J^{\pi} = 1/2^{-}_{1}, 3/2^{-}_{1}, 5/2^{-}_{1}$ and $7/2^{-}_{1}$. The additional use of no-core treatment improves the description of the $9/2^{-}_{1}$ state above the zbm model space although core extensions work adequately but full-core correlation remains essential for precision results. The accuracy of interaction potential selecting along with model space truncation needs improvement because precision degrades in high-energy excitations. Nuclear structure modeling evolves toward fundamental insights about nuclear forces because researchers pick between core-based predictions and fully no-core approaches. This advancement is pivotal in refining our understanding of light nuclei and their role in broader nuclear astrophysics and reaction dynamics.

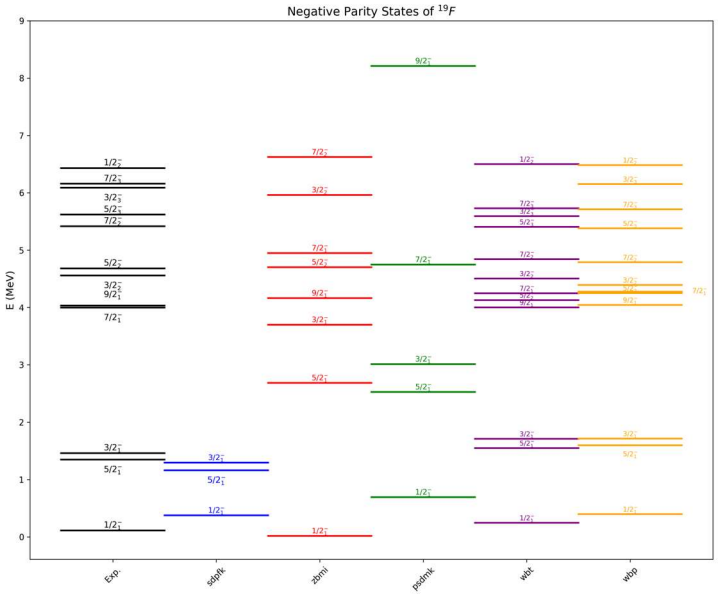

Figure 9. Energy levels of the negative parity states of the $^{19}_{9}F$ nucleus, compared with experimental data obtained from Ref. [22, 29]

3.3. Reduced transition probabilities

In the present study, the calculations of reduced transition probabilities $B(\eta J)$, are carried out using distinct model space interactions. To determine the electric quadrupole $B(E1)$ and magnetic dipole $B(M2)$ transitions among low-lying nuclear states, standard effective charges of $\delta e_p = 0.5$ and $\delta e_n = 0.5$ were applied. One-body density matrices (OBDM) were constructed for the respective model spaces based on their specific interactions. The above technique emphasizes how important it is to use interaction-specific parameters and well-chosen default values when expressing electromagnetic characteristics in nuclear structures.

The reduced transition probabilities $B(J \rightarrow J')$ which compare theoretical predictions from different model spaces and interactions against experimental data for negative parity states of $^{19}_{9}F$ are presented in Table 1. The probability to observe electromagnetic transition between nuclear states is quantified by reduced transition probabilities. The available

experimental values function as reference points to evaluate the predictive ability of multiple nuclear models. Experimental values of the $1/2^+ \rightarrow 1/2^-$ transition yield 0.00055(6) e^2fm^2 as its E1 transition probability, while the $sdpf$ model (SDPFK interaction) computes a value of 0.01190. The transition strength found in zbm (0.005804) and psd (0.003561) is lower than experimental data whereas the WBT and WBP interactions within the $spsdpf$ model yield strongly reduced values indicating decreased probability in the no-core shell model framework.

The E1 transition for $1/2^+ \rightarrow 3/2^-$ demonstrates that the no-core shell model ($spsdpf$) achieves the closest agreement with experimental data compared to other model spaces. Following the no-core approach, the ^4_2He core-based (psd) model also provides a reasonably accurate prediction, further highlighting the impact of extending the model space in refining transition probabilities. Additionally, the M2 transition for $1/2^+ \rightarrow 3/2^-$shows significant deviation between models, with $sdpf$ predicting 7.117, whereas other models yield much smaller values, indicating the sensitivity of M2 transitions to the underlying interaction.

The $1/2^+ \rightarrow 5/2^-$ transitions, particularly for M2 and E3 multipoles, exhibit notable differences among model spaces. The zbm model space (with ZBMI interaction) predicts 255.6 e^2fm^2 for the E3 transition, considerably larger than the $sdpf$ (8.174) and no-core shell model predictions (339 for WBP and 328 for WBT), suggesting an enhanced transition strength with increasing model space complexity. The M4 transition shows significant variations across model spaces, with the $sdpf$ model predicting 438.2, while no-core calculations yield considerably lower values, indicating potential limitations in model truncation or interaction parameterization.

Overall, the Table 1, illustrates the progressive refinement of transition probabilities as model spaces extend from core-based approximations to fully correlated no-core shell model calculations. zbm and $sdpf$ models provide reasonable approximations for low-energy transitions, While the $spsdpf$ model (no-core shell model) demonstrates improved accuracy in capturing multipole transitions, particularly for higher-order electromagnetic transitions (E3, M4, and E5). These results reinforce the importance of model space expansion and interaction refinements in achieving a more comprehensive understanding of nuclear excitation dynamics.

Table 1. Reduced transition probabilities of negative parity states of $^{19}_9F$ compared with experimental [22, 29].

$J_i^\pi \rightarrow J_f^\pi$	$B(\eta J)$ e^2fm^{2J}						
	wL	$Exp.$	$sdpf-sdpfk$	$zbm-zbmi$	$psd-psdmk$	$spsdpf-wbp$	$spsdpf-wbt$
$1/2^+ \rightarrow 1/2^-$	E1	0.00055(6)	0.1190	0.005804	0.003561	0.001919	0.002630
$1/2^+ \rightarrow 3/2^-$	E1	0.0009(2)	0.3007	0.000075284	0.0002681	0.0004784	0.0004972
$1/2^+ \rightarrow 3/2^-$	M2	-	7.117	3.746	0.08010	0.6984	0.5690
$1/2^+ \rightarrow 5/2^-$	M2	-	3.036	0.6826	0.04236	0.08628	0.1853
$1/2^+ \rightarrow 5/2^-$	E3	-	8.174	255.6	259.9	339	327.6
$1/2^+ \rightarrow 7/2^-$	E3	-	145.1	595.1	622.2	64.4	109.6
$1/2^+ \rightarrow 7/2^-$	M4	-	5151	-	7876	4733	5697
$1/2^+ \rightarrow 9/2^-$	M4	-	438.2	-	6.503	14.77	14.62
$1/2^+ \rightarrow 9/2^-$	E5	-	341.8	-	-	302.4	235.9

4. CONCLUSION

The current study explores negative parity states of $^{19}_9F$, showing how transitioning from core-based to no-core shell models improves nuclear structure predictions. The findings highlight those different nuclear properties are optimally reproduced at varying core levels, emphasizing the role of valence nucleons and many-body correlations. For electromagnetic form factors, $sdpf$ model space ($^{16}_8O$ core) provides an initial approximation, but extending to $^{12}_6C$ (zbm model space) significantly improves the C1 and C3 form factors. Further extension to ^4_2He (psd model space) successfully reproduces the E1 and total transverse form factors across the momentum transfer range. The no-core shell model ($spsdpf$) achieves the most accurate results, particularly in resolving initial momentum fluctuations and ensuring consistency in both low- and high-momentum transfer regions. The energy level analysis confirms that core extensions refine predictions, particularly for the $9/2^-$ state. However, the no-core shell model consistently provides the best agreement across all negative-parity states, highlighting the necessity of fully correlated nucleon interactions to capture higher-energy excitations with degree of precision. Reduced transition probability calculations further reinforce the impact of model space selection. While $sdpf$ and zbm models provide reasonable B(E1) and B(M2) values for low-lying transitions, the no-core shell model achieves superior accuracy for higher-order transitions such as E3 and M4. Notably, the ^4_2He-core model space effectively predicts the $1/2^+ \rightarrow 3/2^-$ E1 transition, illustrating that intermediate core choices can yield accurate results for specific states. Overall, this study demonstrates that systematically transitioning from core-based to no-core models optimizes the reproduction of nuclear properties. These findings support nuclear research centers and have direct implications for nuclear astrophysics and reaction dynamics.

ORCID

Berun N. Ghafoor, https://orcid.org/0000-0003-0450-3919

REFERENCES

[1] R. Hofstadter, "Electron scattering and nuclear structure," Reviews of Modern Physics, **28**(3), 214 (1956). https://doi.org/10.1103/RevModPhys.28.21
[2] D. Vautherin, and D.M.T. Brink, "Hartree-Fock calculations with Skyrme's interaction. I. Spherical nuclei," Physical Review C, **5**(3), 626 (1972). https://doi.org/10.1103/PhysRevC.5.626
[3] B.A. Brown, *et al*., "Shell-model analysis of high-resolution data for elastic and inelastic electron scattering on F^{19}," Physical Review C, 32(4), 1127 (1985). https://doi.org/10.1103/PhysRevC.32.1127
[4] T. Sakuda, "Cluster Model Study of Electron Scattering on 19F," Progress of Theoretical Physics, **87**(5), 1159-1169 (1992). https://doi.org/10.1143/ptp/87.5.1159
[5] R.A. Radhi, A.A. Abdullah, and A.H. Raheem, "Calculations of elastic and inelastic electron scattering on ^{19}F using large-basis no core-shell model wave functions," Nuclear Physics A, **798**(1-2), 16-28 (2008). https://doi.org/10.1016/j.nuclphysa.2007.10.010
[6] R.A. Khaleq, *et al*., "Impact of shell model interactions on nuclear responses to WIMP elastic scattering," Physical Review D, **109**(7), 075036 (2024). https://doi.org/10.1103/PhysRevD.109.075036
[7] R.A. Radhi, A.A. Alzubadi, and E.M. Rashed, "Shell model calculations of inelastic electron scattering for positive and negative parity states in ^{19}F," Nuclear Physics A, **947**, 12-25 (2016). https://doi.org/10.1016/j.nuclphysa.2015.12.002
[8] A.P. Zuker, B. Buck, and J.B. McGrory, "Structure of O^{16}," Physical Review Letters, **21**(1), 39 (1968). https://doi.org/10.1103/PhysRevLett.21.39
[9] J.B. McGrory, and B.H. Wildenthal, "Shell-model calculations for A=18, 19, and 20 nuclei with core excitation included explicity," Physical Review C, **7**(3), 974 (1973). https://doi.org/10.1103/PhysRevC.7.974
[10] Y. Utsuno, and S. Chiba, "Multiparticle-multihole states around O 16 and correlation-energy effect on the shell gap," Physical Review C – Nuclear Physics, **83**(2), 021301(R) (2011). https://doi.org/10.1103/PhysRevC.83.021301
[11] B.M. Preedom, and B.H. Wildenthal, "Shell-Model Calculations for Na^{22} and Ne^{22}," Physical Review C, **6**(5), 1633 (1972). https://doi.org/10.1103/PhysRevC.6.1633
[12] S. Cohen, and D. Kurath, "Effective interactions for the 1p shell," Nuclear Physics, **73**(1), 1-24 (1965). https://doi.org/10.1016/0029-5582(65)90148-3
[13] E.K. Warburton, and B.A. Brown, "Effective interactions for the 0p1s0d nuclear shell-model space," Physical Review C, **46**(3), 923 (1992). https://doi.org/10.1103/PhysRevC.46.923
[14] E.K. Warburton, J.A. Becker, and B.A. Brown, "Mass systematics for A= 29–44 nuclei: The deformed A∼ 32 region," Physical Review C, **41**(3), 1147 (1990). https://doi.org/10.1103/PhysRevC.41.1147
[15] B.A. Brown, "Synthesis of mean-field and shell-model configuration-mixing methods," Riken Review, (26), 53-57 (2000).
[16] J.P. Elliott, and T.H.R. Skyrme, "Centre-of-mass effects in the nuclear shell-model," Proceedings of the Royal Society of London Series A. Mathematical and Physical Sciences, **232**(1191), 561-566 (1955). https://doi.org/10.1098/rspa.1955.0239
[17] H. Euteneuer, *et al*., "Elastic electron scattering from the multipole moment distributions of Mg^{25}," Physical Review C, **16**(5), 1703 (1977). https://doi.org/10.1103/PhysRevC.16.1703
[18] T.W. Donnelly, and J.D. Walecka, "Electron scattering and nuclear structure," Annu. Rev. Nucl. Sci. **25**, 329-405 (1975). https://doi.org/10.1146/annurev.ns.25.120175.001553
[19] D. Vautherin, "Hartree-Fock calculations with Skyrme's interaction. II. Axially deformed nuclei," Physical Review C, **7**(1), 296 (1973). https://doi.org/10.1103/PhysRevC.7.296
[20] B.A. Brown, and W.D.M. Rae, "The shell-model code NuShellX@ MSU," Nuclear Data Sheets, **120**, 115-118 (2014). https://doi.org/10.1016/j.nds.2014.07.022
[21] I. Angeli, and K.P. Marinova, "Table of experimental nuclear ground state charge radii: An update," Atomic Data and Nuclear Data Tables, **99**(1), 69-95 (2013). https://doi.org/10.1016/j.adt.2011.12.006
[22] National Nuclear Data Center (NNDC), Brookhaven National Laboratory, Upton, NY 11973-5000, http://www.nndc.bnl.gov/
[23] N.J. Stone, "Table of nuclear magnetic dipole and electric quadrupole moments," Atomic Data and Nuclear Data Tables, **90**(1), 75-176 (2005). https://doi.org/10.1016/j.adt.2005.04.001
[24] N.J. Stone, Table of recommended nuclear magnetic dipole moments. No. INDC (NDS)--0794. International Atomic Energy Agency, 2019.
[25] N.J. Stone, Table of Recommended Nuclear Magnetic Dipole Moments: Part II, Short-Lived States. No. INDC (NDS)--0816. International Atomic Energy Agency, 2020.
[26] K. Kazunari, *et al*., "Shell-model study for neutron-rich sd-shell nuclei," Physical Review C – Nuclear Physics, **83**(1), 014320 (2011). https://doi.org/10.1103/PhysRevC.83.014320
[27] A.J.H. Donné, *et al*., "Elastic magnetic electron scattering from ^{19}F," Nuclear Physics A, **455**(3), 453-476 (1986). https://doi.org/10.1016/0375-9474(86)90317-9
[28] A.J.H. Donné, *et al*., "Transverse electroexcitation of positive-and negative-parity states in ^{19}F," Nuclear Physics A, **469**(3), 518-530 (1987). https://doi.org/10.1016/0375-9474(87)90037-6
[29] D.R. Tilley, *et al*., "Energy levels of light nuclei A= 18–19," Nuclear Physics A, **595**(1), 1-170 (1995). https://doi.org/10.1016/0375-9474(95)00338-1

ПОРІВНЯННЯ МОДЕЛЕЙ З ОСНОВНИМ ТА БЕЗОСНОВНИМ ОБОЛОНКАМИ ПРИ ЗБУДЖЕННІ СТАНІВ ВІД'ЄМНОЇ ПАРНОСТІ $_9{}^{19}$F

Берун Н. Гафур[a,c], Азіз Х. Фатах[b], Арі К. Ахмед[a]
[a]*Університет в Сулеймані, Коледж освіти, Фізичний факультет, Ірак*
[b]*Університет в Сулеймані, Коледж наук, Фізичний факультет, Ірак*
[c]*Науково-дослідний центр, університет в Сулеймані, Ірак*

У цьому дослідженні досліджується ядерна структура низько розташованих станів негативної парності в $^{19}_{9}$F з використанням комбінації оболонкової моделі та методу Хартрі-Фока (HF). Комплексний аналіз ядерних властивостей, включаючи енергетичні спектри, форм-фактори розсіювання електронів, сили переходів, енергії зв'язку та радіуси зарядів, було проведено

в чотирьох модельних просторах: *sdpf*-модельному просторі, *zbm*-моделі, *psd*-моделі та розширеному *spsdpf*-модельному просторі без оболонки. У кожному модельному просторі було застосовано різні ефективні взаємодії для оцінки їхнього впливу на поведінку ядра. Метод HF, що використовує кілька параметризацій Скірма, разом з гармонічним осцилятором та потенціалами Вудса-Саксона, був застосований для обчислення радіальних хвильових функцій одночастинок, необхідних для розрахунків матричних елементів. Результати показують, що розрахунки HF на основі Скірма, при інтеграції з методами моделі оболонки, ефективно фіксують фундаментальні властивості ядра. Систематичне порівняння з експериментальними даними показує, що перехід від модельних просторів з обмеженим ядром до повністю без'ядерної структури значно покращує відтворення форм-факторів розсіювання електронів, особливо в поздовжніх (C1, C3) та поперечних (E1, M2) компонентах. Примітно, що специфічні стани демонструють оптимальну узгодженість на різних рівнях ядра: стани $3/2_1^-$ та $5/2_1^-$ найкраще відтворюються в без ядерній моделі оболонки, тоді як стан $7/2_1^-$ досягає високої точності в модельних просторах zbm та psd. Загалом, це дослідження підкреслює критичний вплив вибору модельного простору та вибору взаємодії в теоретичних ядерних дослідженнях. Поступове уточнення розрахунків від розрахунків на основі ядра до розрахунків без ядра підкреслює роль багаточастинкових кореляцій у ядерних збудженнях та забезпечує глибше розуміння внутрішньої структури $^{19}_{9}F$, сприяючи розвитку теорії структури ядра та динаміки реакцій.

Ключові слова: *структура ядра; модельні простори; core to no-core; Skyrme-HF; фтор-19*